Journal of Materials Chemistry A

Accepted Manuscript

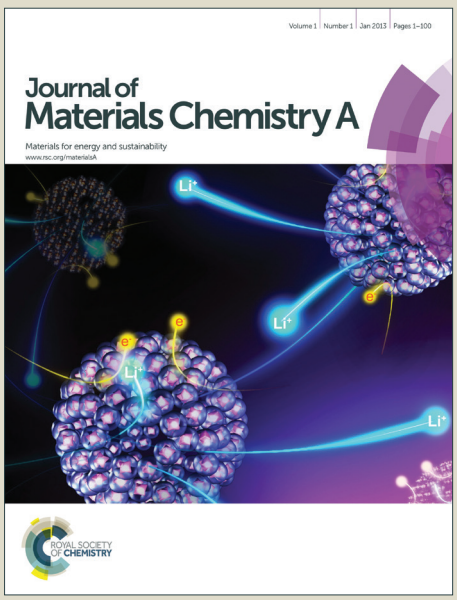

ROYAL SOCIETY OF CHEMISTRY

www.rsc.org/materialsA

Nano-spots Induced Break of Boron Chemical Inertness : A New Route toward Reversible Hydrogen Storage Applications

Martin Depardieu,[1,3] Raphaël Janot,[2*] Clément Sanchez,[3] Hervé Deleuze,[4] Christel Gervais,[3] Marc Birot,[4] Mathieu Morcrette[2] and Rénal Backov[1*]

[1] Université de Bordeaux, Centre de Recherche Paul Pascal, UPR 8641 CNRS, 115 Avenue Albert Schweitzer, 33600 Pessac, France. Email : backov@crpp-bordeaux.cnrs.fr
[2] Laboratoire de Réactivité et Chimie des Solides, UMR 7314 CNRS, Université de Picardie Jules Verne, 33 Rue Saint Leu, 80039 Amiens, France. Email : raphael.janot@u-picardie.fr
[3] Laboratoire de Chimie de la Matière Condensée de Paris, UMR 7574 CNRS, Collège de France, Université Paris 06, Collège de France, 11 Place Marcelin Berthelot, 75231 Paris, France.
[4] Université de Bordeaux, Institut des Sciences Moléculaires, UMR 5255 CNRS, 351 cours de la Libération, 33405 Talence, France

Novel $LiBH_4$-Metal-loaded carbonaceous foams have been designed to trigger reversible hydrogen storage properties. The metallic nanoparticles favour $LiBH_4$ preferential wetting on their surface and subsequent nucleation and growth, a configuration in which borates formation is strongly minimized. A cooperative effect between lower boron oxidation and the presence of metallic particles bearing intrinsic high heat capacity (acting as high temperature nanospots) promotes a strong improvement toward the rehydrogenation process, where boron chemical inertness has been overcome in this way for the first time. Hence, the $LiBH_4$-M@C-HIPE$_{(25HF)}$ hybrid macrocellular foams (with M = Pd or Au) are offering a reversible hydrogen storage process with a remnant capacity of about 7.4 wt% H_2 (related to $LiBH_4$) after 5 desorption/absorption cycles.

Keywords: Hydrogen storage; Foams; Carbon; Colloids; Borohydrides; Integrative chemistry

Energy transportation applications that rely on hydrogen fuel cells are pleading for high capacity reversible hydrogen storage systems. In this context, hydrogen storage in solid-state metal hydrides is extensively investigated because of its high hydrogen storage volumetric capacity at relatively low pressures.[1] More recently borohydrides have attracted much attention due to their high hydrogen contents,[2] features particularly true for $LiBH_4$ when considering its high hydrogen content (18.5 wt%) and good volumetric capacity (121 kg/m^3 H_2). The complete recovery of the whole hydrogen content of $LiBH_4$ remains however difficult as the thermal decomposition of LiH, formed as an intermediate product, occurs at rather high temperatures (above 600 °C under vacuum) thereby limiting the hydrogen release to 13.9 wt%.[2] The simplified decomposition reaction is the following:

$$\mathbf{LiBH_4 \rightarrow LiH + B + 3/2\ H_2} \qquad \mathbf{(1)}$$

Several attempts have been made to increase the kinetic of hydrogen release through catalyst additions.[3] The other strategy to enhance hydrogen release is based on minimizing the $LiBH_4$ particles size by performing its nucleation within a confinement host being either mesoporous silica,[4] or recently mesoporous carbons[5,6] and even more recently macrocellular foams.[7] We were indeed able to tune the hydrogen release of $LiBH_4$ in carbonaceous macrocellular foams by adjusting the walls microporosity, but the rehydrogenation process was still very limited facing the boron chemical inertness.[7] In the present study, we use original micro-macrocellular carbonaceous foams[8] modified with metallic Pd or Au nanoparticles, acting as host sites for the $LiBH_4$ heterogeneous nucleation. This approach leads to the formation of novel carbonaceous foams containing $LiBH_4$, materials labelled "$LiBH_4$-Au/Pd@C-HIPE (*High Internal Phase Emulsion*). The aim of using metallic nanoparticles is to circumvent the boron chemical inertness toward hydrogenation leading to reversible hydrogen storage properties. In this goal, we have first synthesized starting Au/Pd@C-HIPE macroporous

monoliths using Si(HIPE)[9] as hard sacrificial templating matrices. An overall view of their monolithic character, shapes and morphologies can be seen on figure 1, while their full detailed characterizations are addressed within the supplementary section. Basically we can notice that the metal-loaded carbonaceous hosts are macroporous monoliths bearing metallic nanoparticles anchored at the macropores surface.

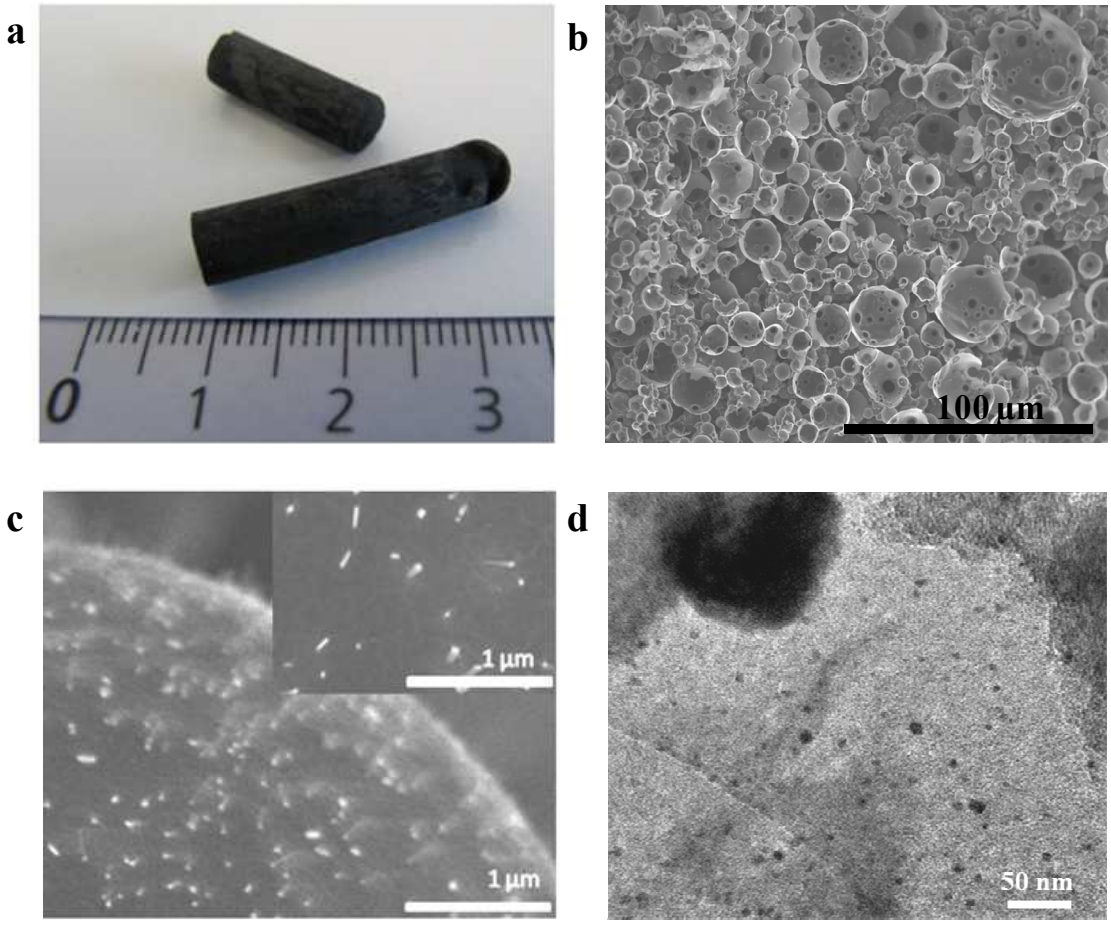

Figure 1. Metal loaded carbonaceous foams overall morphologies. (**a**) Photograph showing the monolithic character of the foams, (**b**) SEM micrograph of the starting C-HIPE$_{(25HF)}$ macrocellular carbonaceous foam, (**c**) SEM micrographs using back-scattered electrons for Au@C-HIPE$_{(25HF)}$. The shiny spots correspond to gold nanoparticles anchored at the macroporous surface, (**d**) Transmission electron microscopy for Au@C-HIPE$_{(25HF)}$.

After the metal loaded carbonaceous foams syntheses and characterization, they were impregnated with $LiBH_4$ and the hydrogen desorption/absorption properties of the hybrid materials were investigated. All the carbon foams were loaded with 20 wt% $LiBH_4$ by the wet

impregnation method using MTBE as solvent as indicated in the experimental part. Figure 2a shows the comparison between XRD diagrams for these composites and commercial $LiBH_4$ (denoted as bulk). Bulk $LiBH_4$ crystallizes in the low-temperature orthorhombic form (*Pnma* space group).[10] The reflections are very sharp indicating the large size of the crystallites and the (200) reflection (at $2\theta_{Cu}$ = 24.6°) is abnormally intense, probably due to a preferential orientation.

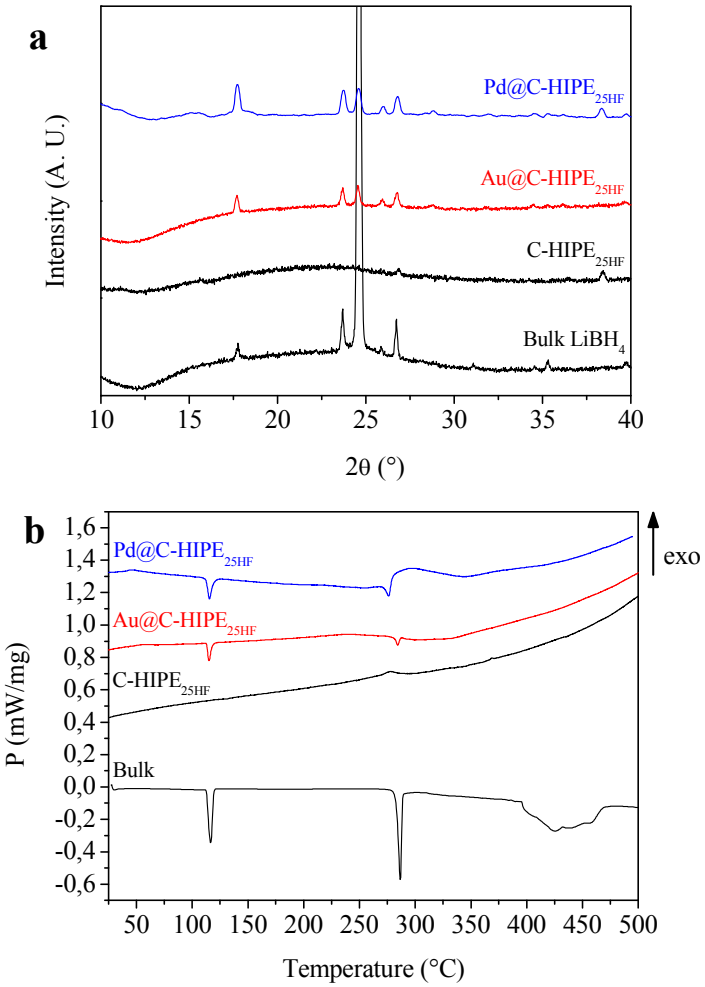

Figure 2. Materials microstructure characterization by XRD and thermodynamic behaviour with temperature through DSC. a) XRD diagrams of bulk $LiBH_4$ and the $LiBH_4$@carbon materials. The $LiBH_4$ loading is about 20 wt% for all the composite materials. **b)** DSC curves under argon of bulk $LiBH_4$ and the $LiBH_4$@carbon materials. The sharp endothermic peaks at 116 and 286 °C are related to structural transition and melting of $LiBH_4$, respectively.

A strong loss of crystalline character is observed when $LiBH_4$ is heterogeneously nucleated on the macrocellular walls of the metallic free C-HIPE$_{(25HF)}$: a complete disappearance of the XRD reflections assigned to $LiBH_4$ is noticed, suggesting either a nucleation into the walls micropores, or the absence of crystallization. Actually, considering the size of the solvent molecules (MTBE, which contains a *tert*-butyl group, is used for the $LiBH_4$ dissolution), there is no way for the nucleation to take place within the 0.5 nm diameter micropores. Therefore, the nucleation probably occurs on the macropores surface, the micropores effect residing in the modification of the macropores walls surface texture, acting as defects. The micropores statistical distribution at the macropores surface is optimizing the nucleation events while minimizing both the $LiBH_4$ growth and crystalline character, as can be seen on the XRD pattern of C-HIPE$_{(25HF)}$ (Figure 2a). The presence of $LiBH_4$ diffraction peaks in $LiBH_4$-Au/Pd@C-HIPE$_{(25HF)}$ sample indicates that the metallic particles favour the crystallization of $LiBH_4$ where the nucleation is minimized while the particle growth is optimized. That is to say the micropores present at the surface of the macroscopic walls of the Au@C-HIPE$_{(25HF)}$ and Pd@C-HIPE$_{(25HF)}$ foams do not dominate the nucleation step anymore. Indeed the carbon walls and the metallic nanoparticles are offering different surface energy, and thereby different wettability toward $LiBH_4$ solutions. The main criteria that governs wettability for low viscosity solutions (bearing viscosity from 1 cP up to 100 cP at 25 °C) is indeed the spreading "S" parameter, indicating the total spreading of a liquid on a solid surface if it is less polarisable than the solid.[11] This is the so-called "wetting criteria" addressed by the Zisman rule.[12] This is mainly the reason why liquid helium will wet and spread over almost everything, bearing an extremely low polarisability. As such, all liquids will easily spread over inorganic glasses (oxide), metals and ionic crystals, these materials having high surface energy. On the other hand, carbon materials that are often bearing surface heteroatoms (mostly oxygen, leading to COOH, OH, COOR groups)[8] that will

minimize their surface energy (being intrinsically already lower than metals surface) will exhibit a lower difference of polarizability between the carbon surface and the electrolyte solute, drastically minimizing the solute wettability. Considering the metallic nanoparticles-modified carbonaceous foams, $LiBH_4$ solution in ether will thereby wet preferentially the metallic nanoparticles and not the carbonaceous walls. Thus, the $LiBH_4$ heterogeneous nucleation will occur preferentially at the metallic surface, but not at the microporous defects of the carbon walls anymore. As there is much less nanoparticles acting as nucleation sites than emerging micropores at the cell surfaces, the nucleation events will be minimized, but the growth optimized to consume the whole $LiBH_4$ precursor molecules.

The loss of $LiBH_4$ crystallinity for the C-HIPE sample prepared with nanoparticle-free carbonaceous foam is confirmed by DSC. The thermal decompositions of the $LiBH_4$@carbon samples, investigated by DSC under argon flow are shown in Figure 2b. For bulk $LiBH_4$, two sharp endothermic peaks at 116 and 286 °C and a very broad endothermic bump above 400 °C can be observed. The first endothermic peak at 116 °C is related to a well-known structural transition between the low-temperature orthorhombic (*Pnma*) and the high-temperature hexagonal ($P6_3mc$) phases of $LiBH_4$,[10] the hexagonal form being largely studied nowadays due to its high Li-ion conductivity (about 10^{-3} S/cm at 130 °C).[13] The second endothermic peak at 286 °C corresponds to the melting of $LiBH_4$ and this molten salt desorbs hydrogen above 400 °C, as revealed by the very broad DSC peak. Actually, the hydrogen desorption of $LiBH_4$ is a complex process involving the formation of intermediate compounds such as $Li_2B_{12}H_{12}$,[14-16] and the hydrogen desorbing flow can be contaminated by the release of volatile species such as diborane (B_2H_6).[4] At 500 °C, the resulting $LiBH_4$ decomposition products are LiH and amorphous boron, the hydrogen desorption of LiH occurring only above 600 °C under vacuum as LiH is a very stable hydride (with an enthalpy of formation of –180 kJ/mol H_2). The shape of the DSC curve is drastically modified for $LiBH_4$@C-HIPE$_{(25HF)}$, where no

peak for structural transition is observed. This is in agreement with the absence of reflections on the corresponding XRD diagram. As the presence of BH_4 group is confirmed by ^{11}B MAS NMR spectroscopy (see below), this suggests that $LiBH_4$ is present as an amorphous phase. Very surprisingly, no endothermic peak of hydrogen release is neither observed for the $LiBH_4$@C-HIPE$_{(25HF)}$ material. On the contrary, a small exothermic peak is detected which can be explained, as discussed in a previous paper,[7] by the penetration of the microporosity and by some irreversible and exothermic reactions with oxygenated groups present at the carbon microporous surface. Even if the carbon matrix has been outgassed under secondary vacuum at 300 °C for 12 h before impregnation, the full removal of chemical groups present in the microporosity is very difficult and these groups are later responsible for the exothermic formation of borates as revealed further by ^{11}B MAS NMR spectroscopy (presence of peaks between 5 and 20 ppm which can be assigned to BO_4 and BO_3 environments).[7] Such strong modification of the DSC curves is not observed when metals are present. The characteristic peaks of $LiBH_4$, for both the structural transition and the melting, are observed at the same temperatures as bulk $LiBH_4$. The hydrogen release appears mildly endothermic, suggesting that no oxidation occurs, which allows to be optimistic for the reversibility and the feasibility of the rehydrogenation reaction. In addition to the DSC analysis, TPD-MS experiments were conducted on the $LiBH_4$@carbon composite materials in order to record their hydrogen release traces (m/z = 2). As shown in Figure 3a, bulk $LiBH_4$ desorbs hydrogen above 300 °C in several steps, the main hydrogen release peak being detected at 445 °C. When $LiBH_4$ is nucleated into the C-HIPE$_{(25HF)}$ matrix, a single sharp peak of hydrogen release is observed at 275 °C, a temperature about 170 °C lower than that of bulk $LiBH_4$. In addition, an extra peak at about 60 °C is also visible and can be attributed to the thermal decomposition of $LiBH_{4-x}(OH)_x$ phases induced by the reaction of $LiBH_4$ with moisture.[17] Due to the strong affinity of the negatively charged hydrogen ($H^{\delta-}$) linked to the B atom and the positively

charged hydrogen ($H^{\delta+}$) of the OH^- group, these hydroxylated phases are easily decomposed and form borates and hydrogen at low temperatures.

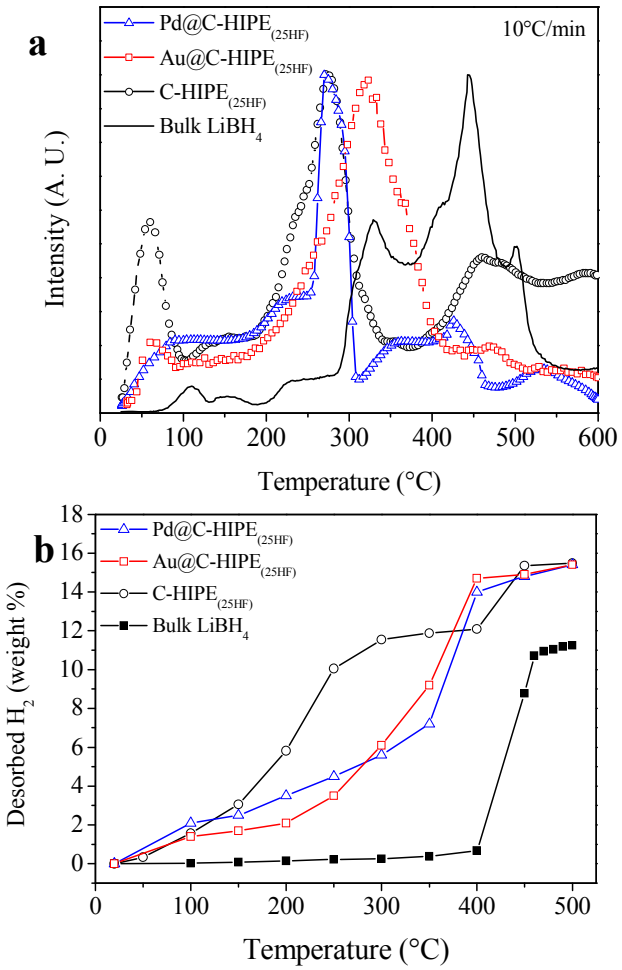

Figure 3. Composites materials hydrogen release with temperature. (**a**) Curves of hydrogen release recorded by mass spectroscopy (*m/z* = 2) for bulk $LiBH_4$ and the $LiBH_4$@carbon materials. The peak seen at 60 °C could be attributed to the thermal decomposition of hydroxylated $LiBH_{4-x}(OH)_x$ phases, (**b**) Amounts of hydrogen release for bulk $LiBH_4$ and the $LiBH_4$@carbon materials measured by the volumetric method.

The peak of hydrogen release at 60 °C is not so intense for the $LiBH_4$-Au/Pd@C-$HIPE_{(25HF)}$ materials, suggesting a less important oxidation, which is confirmed by the DSC curves showing no exothermic reaction at high temperatures. For $LiBH_4$-Pd@C-$HIPE_{(25HF)}$, the main peak of hydrogen release at 275 °C is remarkably sharp, even sharper than that

observed with the same matrix without metallic inclusion. Additional hydrogen release seems to occur above 350 °C, which could correspond to the decomposition of LiH as the TPD-MS experiments were performed under vacuum (P ~ 1 Pa). It is worth mentioning that no other gas release than hydrogen (such as diborane) was detected for the $LiBH_4$@carbon materials on the whole area of investigated temperatures (20–600 °C), whereas borane traces are usually detected for bulk $LiBH_4$. This confirms that the nano-confinement of hydrides is an effective way to suppress, or at least reduce, the contamination as it was already reported in the literature for ammonia-borane[18] or amide-LiH composite materials[19] (with less borazine and ammonia contamination when nano-confined, respectively).

The hydrogen releases of bulk $LiBH_4$, $LiBH_4$@C-HIPE and $LiBH_4$-Pd/Au@C-HIPE samples were quantified by volumetry. The mass fractions of desorbed hydrogen as a function of the temperature are given related to $LiBH_4$ in Figure 3b (these values have therefore to be divided by 5 to know the amount of hydrogen desorbed related to the whole material, *i.e.* including the carbon matrix and the metallic inclusions when present). For bulk $LiBH_4$, the dehydrogenation occurs above 400 °C and reaches 11.2 wt% at 500 °C, which is 81 % of the expected capacity based on the LiH + B formation (theoretical hydrogen release of 13.9 wt%). When $LiBH_4$ is confined in C-HIPE$_{(25HF)}$, the hydrogen release starts below 100 °C. At 300 °C, already 11.6 wt% of hydrogen is desorbed whereas the desorption for bulk $LiBH_4$ is negligible at the same temperature. However, we have to recall that this hydrogen release occurs, at least partially, through irreversible reactions with surface groups of the carbon matrix and that the rehydrogenation will be therefore impossible. At higher temperatures (above 400 °C), a second desorption step is visible, which could account for the thermal decomposition of LiH. The final hydrogen release is very high: a capacity of 15.6 wt% is obtained at 500 °C, which represents about 3.4 H atoms per $LiBH_4$ formula unit. The characterization of the final decomposition products needs further examination as it remains

unclear if Li-B alloys are formed or not. Both $LiBH_4$-Au/Pd@C-HIPE$_{(25HF)}$ materials show similar desorption behaviours (Figure 3) with amounts of hydrogen release smaller below 350 °C than without metallic inclusion, which could be related to the less important oxidation as discussed previously. At 300°C, their hydrogen releases are limited to about 6.0 wt%, whereas that of $LiBH_4$@C-HIPE$_{(25HF)}$ is 11.6 wt%. Above 350 °C, the curves of hydrogen release for the $LiBH_4$-M@C-HIPE materials join that of $LiBH_4$@C-HIPE$_{(25HF)}$ with final hydrogen releases of about 15.5 wt% at 500 °C.

If the enhancement of the hydrogen release of $LiBH_4$ at low temperatures is successfully achieved by balancing the nucleation versus growth rates as demonstrated above, the remaining huge challenge for the use of $LiBH_4$ as hydrogen storage material is still today the rehydrogenation issue. It is very difficult to overcome the boron chemical inertness and the reformation of $LiBH_4$ has been only reported under harsh conditions such as 600 °C and 35 MPa H_2.[20] No catalytic species has been clearly identified to favour the hydrogenation of LiH+B mixture or Li-B alloys and to form $LiBH_4$ under reasonable pressure-temperature conditions. Clearly, the confinement to the nanoscale and the intimate contact between the Li and B atoms could promote the rehydrogenation back to $LiBH_4$. The rehydrogenation of all our materials were performed under 10 MPa H_2 at 400 °C for 12 h. Figure 4 shows the amount of hydrogen released at 500 °C during the first five desorption/absorption cycles for bulk $LiBH_4$ and the $LiBH_4$@carbon materials. Clearly, the rehydrogenation of bulk $LiBH_4$ is impossible in these conditions as no hydrogen is released during the second desorption.[21] Positive effects of confinement on the rehydrogenation were noticed with $LiBH_4$@C-HIPE$_{(25HF)}$, for which a slight hydrogen absorption was observed. This is confirmed when looking at the second desorption as about 2.1 wt% of hydrogen is released. Very interestingly, the inclusion of metallic nanoparticles in the C-HIPE$_{(25HF)}$ matrix greatly improves the rehydrogenation performances. About 10.4 wt% hydrogen is released upon the second

desorption with both Au and Pd inclusions. A reversible process occurs and the retention capacity is slightly better with Pd than with Au. After 5 cycles, the $LiBH_4$-Pd@C-HIPE$_{(25HF)}$ sample still offers a 7.4 wt% hydrogen release (about 48 % of the capacity obtained during the first desorption). As no catalytic effect is reported for Pd or Au particles on the rehydrogenation of $LiBH_4$, the exact mechanism for the improvement of the cyclability of the $LiBH_4$-Pd/Au@C-HIPE$_{(25HF)}$ materials is not yet fully understood, but a scenario can be hypothesized. As observed below from ^{11}B MAS NMR spectra (Figure 5), it is obvious that both Au and Pd metallic nanoparticles improve the rehydrogenation process and promote the formation of BH_4 environment. As said before, the metallic nanoparticles favour $LiBH_4$ localized heterogeneous nucleation and growth on their surface. Upon cycling, the metallic nanoparticles, bearing higher heat capacity than the carbonaceous host foams, are providing higher temperature nanospots where the rehydrogenation kinetic is certainly enhanced.

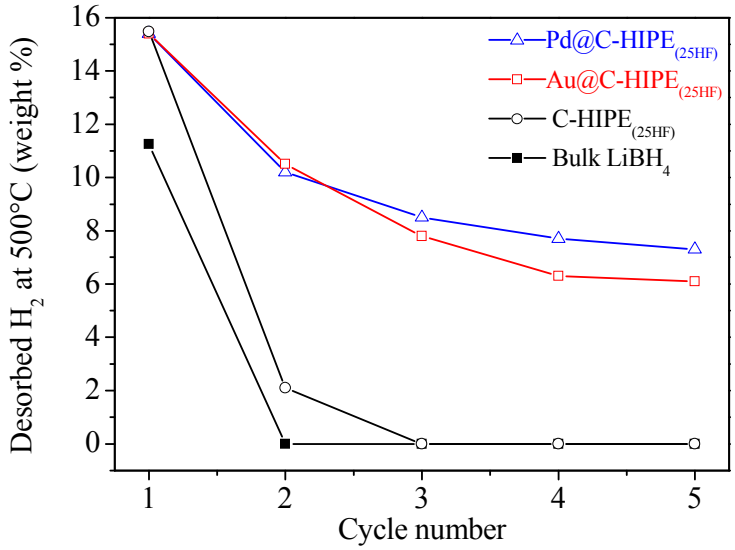

Figure 4. Materials behaviour through hydrogen desorption/adsorption cycles. Amounts of hydrogen released at 500°C for bulk $LiBH_4$ and the $LiBH_4$@carbon materials measured by the volumetric method for the first five cycles. The rehydrogenation is performed under 10 MPa H_2 at 400 °C for 12 h.

^{11}B MAS NMR spectra of bulk $LiBH_4$ and $LiBH_4$@carbon materials are presented in Figure 5. As-prepared materials show a main signal at –41 ppm characteristic of BH_4 environment in $LiBH_4$.

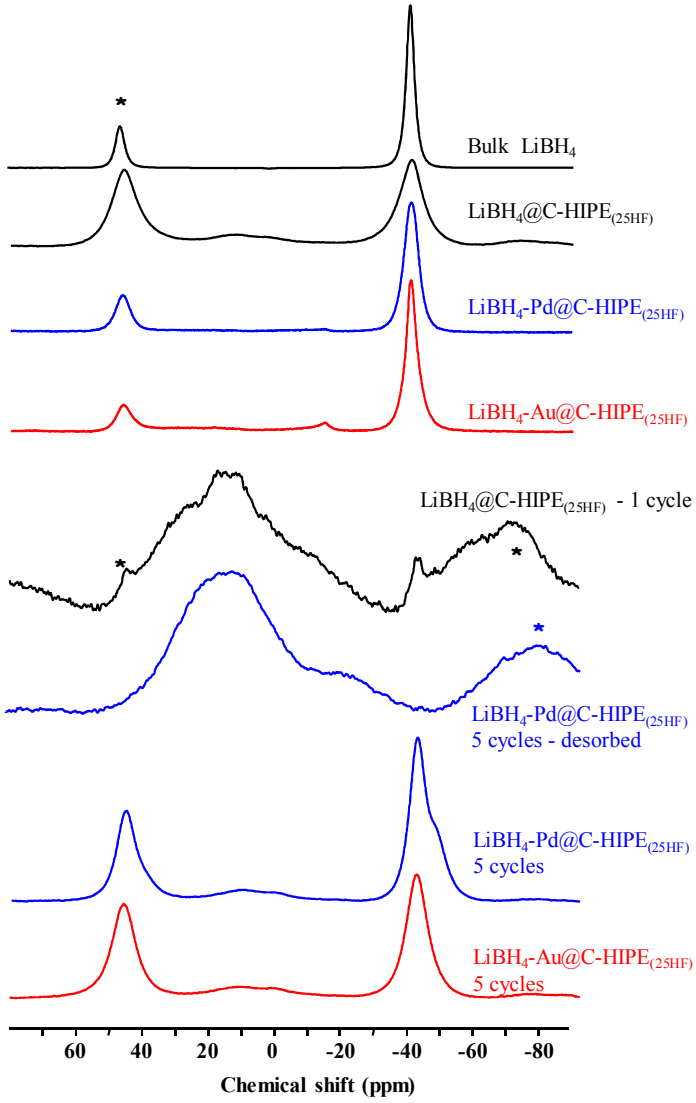

Figure 5. ^{11}B MAS NMR spectra recorded for bulk $LiBH_4$ and the $LiBH_4$@carbon materials. As made, after one or five desorption/absorption cycles and after a sixth desorption (* indicates spinning sidebands).

It can be noticed that this signal is significantly broadened in $LiBH_4$@C-HIPE$_{(25HF)}$ compared to $LiBH_4$-Au/Pd@C-HIPE$_{(25HF)}$ and bulk $LiBH_4$, indicating a loss of crystalline character more important in the absence of metallic particles in agreement with the above

XRD results (Figure 2a). The additional minor signal present at positive chemical shift values in $LiBH_4$@C-HIPE$_{(25HF)}$ and previously assigned to the presence of B-O bonds[7] – due to the interaction of $LiBH_4$ with functional surface groups (-COOH, -OH…) and/or to the reaction of $LiBH_4$ with residual moisture is not present in $LiBH_4$-M@C-HIPE$_{(25HF)}$. This confirms the less important oxidation in metal-containing systems, due to $LiBH_4$ preferential wetting on metallic nanoparticles, as suggested previously by the curves of H_2 release recorded by mass spectroscopy (Figure 3a). After one desorption/absorption cycle, ^{11}B M**AS** NMR spectrum of $LiBH_4$@C-HIPE$_{(25HF)}$ is dominated by a main broad signal ranging from –20 to 40 ppm that can be assigned to amorphous elemental boron[22] confirming the very limited rehydrogenation of the material. In addition, the extra peaks visible at 5 and 20 ppm can be attributed to BO_4 and BO_3 environments and they clearly illustrate the formation of borates, these borates being very stable and not reduced by hydrogen. Therefore, the amount of $LiBH_4$ after one cycle of desorption/absorption is low (*e.g.* only 2.1 wt% of hydrogen is released during the second desorption as shown in Figure 4) and this is confirmed by the small intensity of the peak at –41 ppm. On the contrary, after 5 desorption/absorption cycles, ^{11}B MAS NMR spectra of $LiBH_4$-Au/Pd@C-HIPE$_{(25HF)}$ show a main signal at –41 ppm characteristic of BH_4 environments, confirming that hydrogen recombines with boron and that reversible hydrogen storage process is possible for the $LiBH_4$-M@C-HIPE$_{(25HF)}$ materials. Only the very weak bump between –10 and 20 ppm reveals that some boron does not react with hydrogen and that the process is not fully reversible, but the rehydrogenation performances are by far better than those previously noticed without metallic inclusion. After a 6th desorption, ^{11}B MAS NMR spectra of $LiBH_4$-Pd@C-HIPE$_{(25HF)}$ shows that the $LiBH_4$ signal at –41 ppm has disappeared while a composite signal with two broad components centred at ~15 and ~ –20 ppm has appeared. The first one can be assigned to amorphous boron while the second could correspond to $Li_2B_{12}H_{12}$[22a] or a related species. ^{6}Li and ^{7}Li MAS NMR spectra (Figure S8,

supplemental) were also recorded to confirm these attributions, showing for $LiBH_4$-Au/Pd@C-HIPE$_{(25HF)}$ compounds a signal at –1.3 ppm characteristic of $LiBH_4$.[22a,23] In the case of M = Pd, an additional signal is observed at more negative chemical shift values, as observed on the ^{11}B spectrum. Such a splitting of the line shape in two components has already been reported for $LiBH_4$ confined in porous carbon and ordered porous silica[24] and was assigned to enhanced mobility of BH_4^- and Li^+ due to confinement. In our case, there is no particularly narrow line observed that could confirm this mobility but this phenomenon may be hidden by the broadening of the lines due to anisotropic susceptibility effects induced by the carbon host. It should be noticed that there is no obvious signal around 0 ppm where LiH environments are expected.[22a,25] Nonetheless, the ^6Li LiH signal is difficult to observe due to both its long relaxation time and the broadness of the ^7Li peak induced by stronger quadrupolar interactions. After desorption, a peak centred at –0.6 ppm is observed on the Li spectra of $LiBH_4$-Pd@C-HIPE$_{(25HF)}$ that can be attributed to $Li_2B_{12}H_{12}$[23b] in good agreement with the ^{11}B NMR results. Li metal resonance has been reported at ~ 250 ppm,[26] this large shift value being caused by the Knight shift. This region has been explored both by ^6Li and ^7Li NMR but no signal was observed for desorbed $LiBH_4$-Pd@C-HIPE$_{(25HF)}$, indicating the absence of metallic lithium after desorption. This could suggest that some Li-B alloys are formed.

In conclusion, macrocellular carbonaceous foams bearing metallic nanoparticles inclusions of Pd/Au have been synthesized and used as host matrices for lithium borohydride ($LiBH_4$) confinement. The synthetic path involved first the synthesis of siliceous foams obtained through combining direct concentrated emulsions with sol-gel chemistry. In a second step these foams were employed as hard templates for the morphogenesis of carbonaceous foams[7] where metallic nanoparticles were subsequently heterogeneously nucleated. These host matrices were then impregnated by a wet method using $LiBH_4$ solvated in ethers, which

led to the generation of $LiBH_4$-Au/Pd@C-HIPE$_{(25HF)}$ hybrid macrocellular foams with a $LiBH_4$ loading of 20 wt%. Compared to previous results with metallic-free carbonaceous foams, borates formation is much reduced, which can be explained by the wetting-induced preferential nucleation of $LiBH_4$ on the metallic particles. This configuration that lower boron oxidation during dehydrogenation, combined with the metallic particles intrinsic high heat capacity (acting as high temperature nanospots), allows a strong improvement of the rehydrogenation process. As such, the $LiBH_4$-Au/Pd@C-HIPE$_{(25HF)}$ hybrid materials propose reversible hydrogen storage process at 400 °C with still a capacity of about 7.4 wt% (related to $LiBH_4$ meaning 1.5 wt% for the total weight of the sample including carbon and metallic inclusions) after 5 desorption/absorption cycles. If the enhancement of the hydrogen release kinetic of $LiBH_4$ by confinement into porous carbons is well reported in the literature,[27-28] there are only few reports about the rehydrogenation performances. For $LiBH_4$ confined in carbon aerogels,[5] the hydrogen desorption capacity was reported to be only 1.2 % after 3 cycles at 400°C showing therefore a lower cyclability than that demonstrated here for the $LiBH_4$-Au/Pd@C-HIPE$_{(25HF)}$ hybrid materials.

Hence, these novel $LiBH_4$-metal-loaded carbonaceous foams constitute yet another example of how the integrative chemistry[29] synthetic path allows the design of new materials bearing promising property. Beyond the reversible hydrogen storage property, it is also the first time that boron chemical inertness toward hydrogenation is circumvented by using metallic nanoparticles without nano-confinement. Due to the high cost of Au and Pd, the large scale utilisation for such hybrid materials is poorly probable, but we have no doubt that much cheaper metallic inclusions could also promote the boron hydrogenation. This feature will certainly drive new opening toward both energy storage process and heterogeneous catalysis where boron atoms are involved.

Experimental section

Materials. Tetraethoxysilane ($Si(OEt)_4$, TEOS), purity >99 %; dodecane, purity >90 %; palladium chloride ($PdCl_2$), and potassium tetrachloroaurate ($KAuCl_4$) were purchased from Sigma-Aldrich. Cetyltrimethylammonium bromide ($((C_{16}H_{33})N(CH_3)_3Br$, CTAB), purity 98 %, was purchased from ChemPur. Hydrochloric acid, 37 %, was purchased from Carlo Erba Reagents. Ablaphene RS101 (formophenolic prepolymer resin of the resol type in a hydroalcoholic solution) was purchased from Rhodia. All chemicals were used as received without further purification.

Macrocellular silica hard template synthesis (Si-HIPE).

The silica hard template is a typical Si-HIPE, for which the synthesis from the combination of sol-gel chemistry and a concentrated emulsion has already been studied and described elsewhere.[8] Typically, TEOS (5 g) is added to an acidified concentrated CTAB solution (16 g of 35 wt% CTAB in water with 6 g HCl). The solution is hand stirred until it becomes transparent as the TEOS is hydrolyzed. The solution is then poured into a mortar and dodecane (35 g) is added drop by drop while stirring slowly with a pestle. After the last drop of dodecane, stirring is maintained for a few seconds to assure the absence of visible dodecane drops in the concentrated emulsion and its homogeneity. This emulsion is then poured into moulds – in this case polystyrene test tubes – and is left to rest for a week while the condensation reactions take place. Drying at this stage is to be avoided, so the tubes are either closed or put under a saturated water/ethanol atmosphere. After condensation, the samples are put in a 1:1 THF/acetone mix three times for 24 h to eliminate dodecane. They are then slowly dried in a desiccator over a few days. After drying, the Si-HIPE are calcinated at 650 °C for 6 h with a heating rate of 2 °C/min and a first plateau at 200 °C for 2 h to eliminate surfactant residues.

Macrocellular carbon synthesis (C-HIPE).

The overall macro-microcellular foams synthetic paths are described elsewhere.[8] Typically, Si-HIPE monoliths are immerged in a beaker containing a solution composed of 25 wt% phenolic resin in THF (hence the name 25HF). The beakers are placed under a dynamic vacuum until the effervescence, from the air removal from the silica foams, stops. The system is then put under a static vacuum for three days. The samples are rapidly rinsed with THF and then placed at 80 °C for 24 h into an oven to initiate resin polymerization. To complete the polymerization, a thermal treatment in air at 155 °C for 5 h is applied with a heating rate of 2 °C/min with a first plateau at 80 °C for 12 h followed by a second one at 110 °C for 3 h. Pyrolysis is performed at 900 °C for 1 h, with a heating rate of 4 °C/min. Silica hard templates are removed by washing the samples with a 10 % HF solution for 24 h, which is eliminated by rinsing three times for 24 h in distilled water.

Palladium nanoparticles heterogeneous nucleation.

C-HIPE are put in a beaker containing a 4.5×10^{-2} M solution of $PdCl_2$ in a 1:1 acetone/water mix acidified with 0.5 mL HCl. The beaker is put under a dynamic vacuum until foam disappearance and, then, put under a static vacuum for three days. The samples are dried in air and, then, $PdCl_2$ is reduced by a thermal treatment at 400 °C (heating rate 2 °C/min) under hydrogen. These samples are labelled hereafter as Pd@C-HIPE$_{(25HF)}$.

Gold nanoparticles heterogeneous nucleation.

C-HIPE are put in a beaker containing a 4.5×10^{-2} M solution of $KAuCl_4$ in a 1:1 acetone/water mix. The beaker is put under a dynamic vacuum until foam disappearance and, then, let under a static vacuum for three days. The samples are dried in air and, then, Au^{3+} is reduced by a thermal treatment at 80 °C under 0.8 MPa of H_2. These samples are labelled hereafter as Au@C-HIPE$_{(25HF)}$.

$LiBH_4$-Au@C-HIPE$_{(25HF)}$ and $LiBH_4$-Pd@C-HIPE$_{(25HF)}$ syntheses.

Considering the material metallic nanoparticles free $LiBH_4$@C-HIPE$_{(25HF)}$, its synthesis can be found elsewhere.[7] All transformations with $LiBH_4$ is performed within glove box under purified Ar atmosphere. A 0.1 M $LiBH_4$ solution is first obtained through dissolution of 217 mg of $LiBH_4$ powder into 100 mL of methyl *tert*-butyl ether (MTBE, $C_5H_{12}O$, Sigma–Aldrich, > 99.8%, previously dried and kept over molecular sieves) at ambient temperature and vigorous stirring. The carbonaceous hosts are outgassed at 300 °C under secondary vacuum ($P < 10^{-2}$ Pa) for 12 h before $LiBH_4$ impregnation. Final impregnated carbonaceous foams are then extracted from the media using a filtration process and then dried under primary vacuum at ambient temperature. Several cycles of impregnation/drying were performed in order to optimize the $LiBH_4$ content embedded into the carbonaceous host. The loading in $LiBH_4$ of the samples was deduced from the measurements of Li contents. Known weights of samples were dissolved in an acidic solution (1.0 M HCl) under vigorous stirring. Atomic absorption spectroscopy (PerkinElmer Analyst 300) determined the Li contents of the resulting solutions. Standard solutions of 1, 2 and 3 mg/L were initially used for the Li calibration of the spectrometer. Final carbonaceous materials are labelled hereafter as $LiBH_4$-Au@C-HIPE$_{(25HF)}$ and $LiBH_4$-Pd@C-HIPE$_{(25HF)}$.

Characterization. Scanning electron microscopy (SEM) observations were performed with a Hitachi TM-1000 apparatus at 15 kV. The specimens were gold-palladium-coated in a vacuum evaporator prior to examination. High-resolution transmission electron microscopy (HR-TEM) micrographs were obtained with a Jeol 2200 FS microscope. The samples were ground into powders that were then deposited on a copper grid coated with a Formvar/carbon membrane. Surface areas and pore characteristics on a micro-(meso)scale were obtained with a Micromeritics ASAP 2010 apparatus. Intrusion/extrusion mercury measurements were performed using a Micromeritics Autopore IV 9500 porosimeter, this to reach the scaffolds macrocellular cells characteristics. The samples were studied by X-ray diffraction (XRD)

using a Bruker D8 diffractometer (Cu K_α radiation, λ = 1.54056 Å) equipped with a position sensitive detector (PSD). Due to the reactivity with air and moisture of highly divided $LiBH_4$, an air-tightened sample holder with a beryllium window was used. Calorimetric measurements were carried out by differential scanning calorimetry (Netzsch DSC 204) under argon flow (100 mL/min) using sealed stainless steel crucibles with caps being perforated immediately before the analysis to allow gas releases upon heating. A heating rate of 2 °C/min was used for all experiments. TPD-MS experiments (temperature-programmed desorption coupled with a mass spectrometer) were carried out on neat $LiBH_4$ and $LiBH_4$@carbon materials with a quadripolar mass spectrometer QXK300 (VG Scientific Ltd.). The procedure consisted in loading about 5 mg of powder in a stainless steel tube (6 mm in diameter). The tube was then connected to the mass spectrometer and outgassed under a primary vacuum (1 Pa). The TPD curves (m/z = 2 for hydrogen) were acquired at a heating rate of 10 °C/min and temperatures up to 600 °C. The hydrogen desorption was followed by volumetric measurements using a homemade Sievert type instrument. After outgassing at room temperature, the hydrogen absorption/desorption properties of the sample were calculated from the pressure changes in calibrated volumes using the ideal gas law. The hydrogen desorption capacity was measured every 50 °C from 50 to 500 °C. For each temperature, the measurement of the hydrogen desorption capacity was made after a total release duration of 2 h. The calibrated volume, in which hydrogen was collected, was regularly emptied in order to have always a pressure below 0.1 MPa. The samples were rehydrogenated under 10 MPa H_2 at 400 °C for 12 h. ^{11}B and ^{7}Li MAS NMR spectra were recorded at 11.75 T on a Bruker Avance 500 wide-bore spectrometer operating at 128.28 and 194.38 MHz respectively, using a Bruker 4 mm probe and a spinning frequency of the rotor of 14 kHz. ^{6}Li MAS NMR spectra were recorded at 16.3 T (103.01 MHz) on a Bruker Avance 700 standard-bore spectrometer using a spinning frequency of 14 kHz. The ^{6}Li and ^{7}Li spectra

were acquired with a short single pulse acquisition with a small nutation angle ($\pi/12$) while ^{11}B spectra were acquired using a spin-echo $\theta–\tau–2\theta$ pulse sequence with $\theta = 90°$ to overcome problems of probe signal. The τ delay was synchronized with the spinning frequency. Recycle delays of 1 s were used for ^{11}B and ^{7}Li while much longer ones (typically 800 s) were applied for ^{6}Li presenting very long relaxation times (T_1). Chemical shifts were referenced to BF_3:OEt_2 for ^{11}B and 1.0 M LiCl aqueous solution for ^{6}Li and ^{7}Li ($\delta = 0$ ppm).

References

1 Züttel, A. *Mater. Today* 2003, 24.
2 (*a*) Züttel, A.; Rentsch, S.; Fischer, P.; Wenger, P.; Sudan, P.; Mauron, P.; C. Emmenegger, C. *J. Alloys Compd*. 2003, *356–357*, 515. (*b*) Züttel, A.; Borgschulte, A.; Orimo, S. *Scripta Mater*. 2007, *56*, 823.
3 Au, M. ; Jurgensen, A. *J. Phys. Chem. B* 2006, *110*, 7062.
4 Kostka, J.; Lohstroh, W.; Fichtner, M.; Hahn, H., *J. Phys. Chem. C* 2007, *111,* 14026.
5 Gross, A.; Vajo, J.; Van Atta, S.; Olson, G., *J. Phys. Chem. C* 2008, *112*, 5651.
6 Cahen, S.; Eymery, J.-B.; Janot, R.; Tarascon, J.-M. *J. Power Sources* 2009, *189*, 902.
7 Brun, N; Janot, R.; Gervais, C.; Morcrette, M.; Deleuze, H.; Sanchez, C.; Backov, R. *Energy & Environmental Science*, 2010, *3*, 824.
8 *(a)* Brun, N.; Prabaharan, S.R.S.; Morcrette, M.; Sanchez, C.; Pécastaing, G.; Derré, A.; Soum, A.; Deleuze, H.; Birot, M.; Backov, R. *Adv. Funct. Mater*, 2009, *19,* 3136. *(b)* Brun, N.; Prabaharan, S.R.S.; Morcrette, M.; Deleuze, H.; Birot, M.; Babot, O.; Achard, M.-F.; Surcin, C.; Backov, R. *J. Phys. Chem. C*, 2012, *116*, 1408.
9 Carn, F.; Colin, A.; Achard, M.-F.; Deleuze, H.; Birot, M.; Backov, R. *J. Mater. Chem.* 2004, *14*, 1370.
10. Soulié, J.P.; Renaudin, G.; Cerny, R.; Yvon, K. *J. Alloys Compd.* 2002, 346, 200.
11. de Gennes, P. G.; Brochar-Wyart, F. Quéré, D. in "*Gouttes, bulles, perles et ondes*", collection échelles, Belin Edition 2005.
12. (*a*) Zisman, W. in "*Contact angle wettability and adhesion*", Chemical series, 1964, 43, Washington. (*b*) Fox, J.; Zisman, W. *J. Colloid Interface Sci*. 1950, 5, 514.
13. Matsuo, M.; Nakamori, Y.; Orimo, S.; Maekawa, H.; Takamura, H.; *Applied Phys. Let.* 2007, 91, 224103.
14. Orimo, S.; Nakamori, Y.; Ohba, N.; Miwa, K.; Aoki, M.; Towata, S.; Züttel, A. *Appl. Phys. Lett.* 2006, 89, 219201.
15. Hwang, S-J.; Bowman, R.C.; Reiter, J. W., Rijssenbeek, J.; Soloveichik, G.L.; Zhao, J-C.; Kabbour, H.; Ahn, C.; *J. Phys. Chem. C,* 2008, 112, 3165
16. Friedrichs, O.; Remhof, A.; Hwang, S-J.; Züttel; A.; *Chem. Mater.* 2010, 22, 3265
17. Mosegaard, L.; Moller, B.; Jorgensen, E.; Bösenberg, U.; Dornheim, M.; Hanson, J.; Cerenius, Y.; Walker, G.; Jakobsen, H.; Besenbacher, F.; Jensen, T. *J. Alloys Compd.* 2007, 446-447, 301.

18. Gutowska, A. ; Li, L.Y.; Shin, Y.S.; Wang, C.M.; Li, X.H.; Linehan, J.C.; Smith, R.S.; Kay, B.D.; Schmid, B.; Shaw, W.; Gutowski, M.; Autrey, T. *Angew. Chem., Int. Ed.,* 2005, 44, 3578.
19. Demir-Cakan, R.; Tang, W.S.; Darwiche, A.; Janot, R. *Energy Environ. Sci.* 2011, 4, 3625.
20. Orimo, S.; Nakamori, Y.; Kitahara, G.; Miwa, K.; Ohba, N.; Towata, S.; Züttel, A. *J. Alloys Compd.* 2005, 427, 404.
21. Mauron, P.; Butcher, F.; Friedrichs, O.; Remhof, A.; Bielmann, M.; Zwicky, C.N.; Züttel, A. *J. Phys. chem B* 2008, 112, 906.
22. (*a*) Choi, Y.J.; Lu, J.; Sohn, H.Y.; Fang, Z.Z.; Kim, C.; Bowman, R. C.; Hwang, S.-J. *J. Phys. Chem. C* 2011, *115*, 6048. (*b*) Yan, Y.; Remhof, A.; Hwang, S.-J.; Li, H.-W.; Mauron, P.; Orimo , S.-I.; Züttel, A. *Phys. Chem. Chem. Phys.* 2012, *14*, 6514.
23. (*a*) Kim, C.; Hwang, S.-J.; Bowman, R.C.; Reiter, J.W.; Zan, J.A.; Kulleck, J.G; Kabbour, H.; Majzoub, E.H.; V. Ozolins, V. *J. Phys. Chem. C* 2009, 113, 9956. (*b*) Purewal, J.; Hwang, S.-J.; Bowman, R.C.; Ro□nnebro, E.; Fultz, B.; Ahn, C. *J. Phys. Chem. C* 2008, 112, 8481.
24. Verkuijlen, M.H.W.; Ngene, P.; de Kort, D.W.; Barre, C.; Nale, A.; van Eck, E.R.H.; van Bentum, P.J.M., de Jongh, P.E.; Kentgens, A.P.M. *J. Phys. Chem. C* 2012, 116, 22169.
25. (*a*) Hu, J.Z.; Kwak, J.H.; Yang, Z.; Wan, X.; Shaw, L.L. *Journal of Power Sources* 2010, 195, 3645. (*b*) Shaw, L.L.; Wan, X.; Hu, J.Z.; Kwak, H.; Yang, Z. *J. Phys. Chem. C* 2010, 114, 8089.
26. Bhattacharyya, R.; Key, B.; Chen, H.; Best, A.S.; Hollenkamp, A.F.; Grey, C.P. *Nature Mat.* 2010, 9, 504.
27. de Jongh, P.E.; Adelhelm, P. *Chem. Sus. Chem.* 2010, 3, 1332.
28. Vajo, J.J. *Curr. Opin. Solid State Mat. Sci.* 2011, 15, 52.
29. (*a*) Backov, R. *Soft Mater* 2006, *2*, 452. (*b*) Brun, N.; Ungureanu, S.; Deleuze, H.; Backov, R.; *Chem. Soc. Rev.*, 2011, 40 , 771. (*c*) Sanchez, C.; Belleville, P.; Popall, M.; Nicole, L. *Chem. Soc. Rev*. 2011, 40, 696.

Acknowledgements
The authors wish to thank Eric Lebraud from ICMCB for the XRD experiments and Elisabeth Sellier from CREMEM for the HR-TEM experiments. The French Région Ile-de-France SESAME program is acknowledged for financial support (700 MHz spectrometer).

Supplemental information available.

TOC

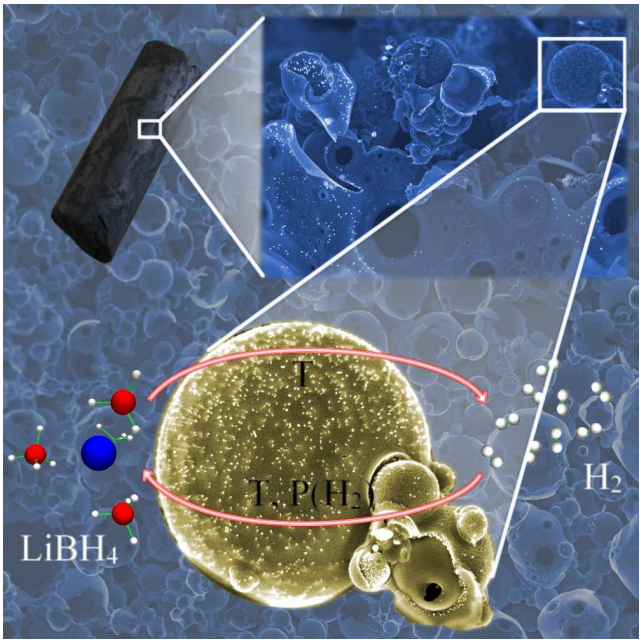

Macrocellular carbonaceous foams bearing metallic nanoparticles inclusions of Pd/Au have been designed to trigger lithium borohydride ($LiBH_4$) reversible hydrogen storage properties.